NJC

ROYAL SOCIETY OF CHEMISTRY

COMMUNICATION

View Article Online
View Journal

Cite this: DOI: 10.1039/d1nj00660f

Received 8th February 2021,
Accepted 15th April 2021

DOI: 10.1039/d1nj00660f

rsc.li/njc

Unexpected radical mechanism in a [4+1] cycloaddition reaction†

István Bors,[a] Mihály Purgel,[b] Péter Pál Fehér,[c] Tamás Varga,[d] Gábor Speier,[a] László Korecz[e] and József Kaizer*[a]

9,10-Phenanthrenequinone monoimines (2,7-R-PQI, R = *t*Bu, H, Br, NO_2, 1a–d) undergo a [4+1] cycloaddition reaction with triphenylphosphine to give 2,3-dihydro-2,2,2-triphenylphenanthro[9,10-*d*]-1,3,2λ^5-oxazaphospholes (3a–d). During the reaction, highly colored radicals are formed as intermediates, which were characterized by EPR and UV-vis spectroscopy. The formation rate and the rate of decay of these radicals were determined kinetically. These radicals exhibit high persistency and under inert conditions can be handled conveniently. Based on detailed kinetic and spectroscopic studies and DFT calculations, a plausible mechanism has been proposed.

Although electrocyclic reactions, in general, attract intense interest, [4+1] cycloaddition (or cheletropic) reactions are somewhat outside of this scope.[1] Trivalent phosphorus compounds[2] readily undergo additions with 1,4-dioxa-1,3-dienes (*o*-quinones), and in these cases a concerted reaction mechanism has been assumed.[3] It was observed that *o*-quinone monoimines (**1a–d**) readily react with triphenylphosphine in a cheletropic reaction to 2,3-dihydro-2,2,2-triphenylphenanthro [9,10-*d*]-1,3,2-λ^5-oxazaphospholes (**3a–d**) (eqn (1)),[4] which serve as good bioinspired organocatalysts for the oxidation of thiophenol, cysteine, and glutathione to their disulfides,[5] triphenylphosphine to triphenylphosphine oxide,[6] 3,5-di-*tert*-butylcatechol to the corresponding *o*-quinone and 2-aminophenol to 2-aminophenoxazine-3-one by molecular oxygen.[7]

During the synthesis of **3**, we have observed that the color of the solution mixtures turns to deep red, which fades at the end of the reaction to give pale yellow end products (Fig. 1). The presence of radical species was suspected and a more detailed investigation of the reaction was undertaken.

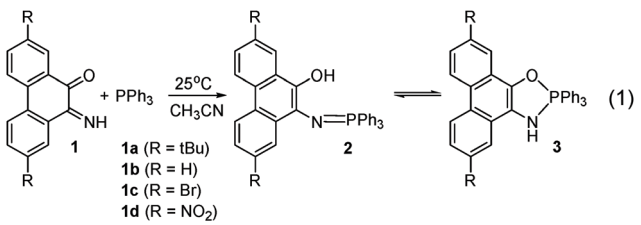

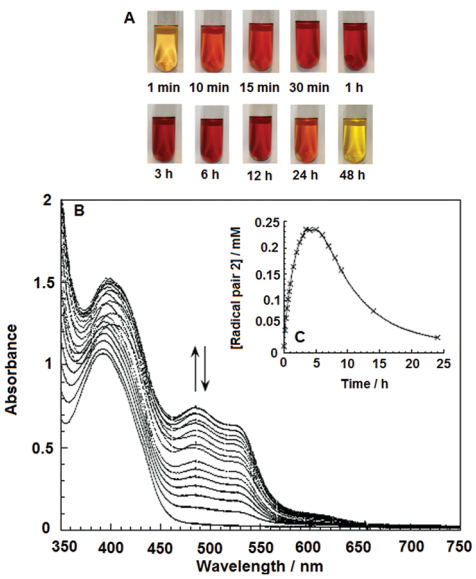

Fig. 1 Color (**A**) and visible spectral change during the reaction of 9,10-phenanthrenequinone monoimine **1b** (0.5 mM) and triphenylphosphine (0.5 mM) (**B**). Inset: Time course of formation and decay of the radical intermediate from **1b** and triphenylphosphine in 10 mL acetonitrile at 50 °C under Ar (**C**).

[a] *Research Group of Bioorganic and Biocoordination Chemistry, University of Pannonia, Veszprém H-8200, Hungary. E-mail: kaizer@almos.uni-pannon.hu*
[b] *Department of Physical Chemistry, University of Debrecen, Debrecen H-4032, Hungary*
[c] *Institute of Organic Chemistry, Research Centre for Natural Sciences, Budapest H-1117, Hungary*
[d] *Department of Process Engineering, University of Pannonia, Veszprém H-8200, Hungary*
[e] *Institute of Materials and Environmental Chemistry, Research Centre for Natural Sciences, Budapest H-1117, Hungary*

† Electronic supplementary information (ESI) available: Additional spectroscopic and kinetic data, synthetic procedures and characterisation. See DOI: 10.1039/d1nj00660f

Mixing 0.5 mM solutions of 9,10-phenanthrenequinone monoimine **1b** and triphenylphosphine (0.5 mM) in acetonitrile at 50 °C under argon gives in *ca.* 0.5–1 h intense red solutions (Fig. 1A).

The formation and decay of the red compound were followed by UV-vis spectroscopy. In addition to the absorption of **1b** [λ_{max} (ε) 216 (22 101), 263 (29 335), 313 (3706), 395 (1778 mol^{-1} L cm^{-1}) nm], new absorption bands at 524 and 486 nm appeared with time (Fig. 1B). These peaks reached maxima after 5 h and almost disappeared after 24 h (Fig. 1C). A similar spectrum was observed from the reaction of **3b** and TEMPO resulting in the oxazaphospholyl radicals (**2b**$^{\bullet}$ or **3b**$^{\bullet}$), which can be used for the calculation of the radical concentration using a calibration curve (Fig. S1, ESI† [λ_{max} (ε) 486 (3154 mol^{-1} L cm^{-1}) nm]). After two days the solution was pale yellow. That means that the formation of the radical species is faster than its reaction to the end product and that is responsible for the enrichment of the proposed oxazaphospholyl radical with **1b** based on the stoichiometry of the reaction above (Fig. 1C). DFT mechanistic study and TDDFT calculations predicted stable radical pairs (RP1 and RP2) consisting of **2b**$^{\bullet}$ and PQIH$^{\bullet}$, whose spectrum showed good agreement with the experimental one; see below and the ESI.† However, the EPR spectra of the radicals formed in the case of compounds **1a–d** are almost perfectly symmetrical (Fig. 2 and Fig. S2–S4, ESI†) suggesting that the observed spectra cannot be signals of the **RP**. In the case of weak coupling or no coupling, the spectrum would be a superimposed spectra of the two different radicals with different g values, which cannot give a symmetric spectrum. The case of strong coupling is more complicated but, based on similar symmetry considerations, the case of the radical pair is almost ruled out. It is worth noting that almost identical kinetic runs were observed following the reaction by parallel UV-vis and EPR measurements (Fig. S5, ESI†). Density functional theory (DFT) computations were performed for radicals originating from compounds **1a–d** using the ORCA package.[8] Using the results of DFT calculations as a starting point, simulations of the spectra were carried out by using EPR software to identify the radicals.[9] The EPR spectra can be simulated by assuming one phosphorus and one nitrogen atom as well as eight protons for the **1b** and six protons for the disubstituted **1a,c,d** derived radicals. In addition, two different ^{13}C couplings were taken into account in the simulations, but unfortunately the determination of the exact number of atoms belonging to each coupling was not allowed by the relatively broad linewidth. The comparison of hyperfine coupling helps to assign the couplings in positions 2 and 7. We assume that radical **2b**$^{\bullet}$ or **3b**$^{\bullet}$ (or both) is the source of the obtained EPR signal. Different sets of hyperfine coupling constants can provide simulations of almost the same quality due to the relatively low resolution. Nitrogen and two almost equivalent protons have a very similar effect on the spectra so their hyperfine coupling constants are interchangeable if the resolution is not good enough. The agreement between the DFT calculations and the EPR parameters determined from the spectra is adequate and only the nitrogen coupling is overestimated by the DFT calculation. DFT geometry optimization for free radicals, both closed and open ring, always resulted in the open ring geometry contrary to closed-shell systems. Hence, we identify the radical as open ring **2b**$^{\bullet}$. The unique situation that only radical **2b**$^{\bullet}$ could be seen in the EPR spectra suggests that the radical species (PQIH$^{\bullet}$) formed during the reaction are planar and probably stacked in solution and so undergo intermolecular interactions to render them EPR-silent.[10] Isoelectronic 9,10-phenanthrenequinone semiquinone radical anions tend to interact in this manner generally and the separation of nearly parallel aligned semiquinone ligands in [Cu(9,10-PSQ)(PPh_3)]$_2$ of 2.8 Å suggests π–π interactions between the highly delocalized π-system rings.[10] The cyclic voltammograms (CVs) display reversible oxidation waves in the case of 1,3,2-oxazaphospholes (**3a–d**) and irreversible waves (**1a–d**) in the case of imines.

The substituted 9,10-phenanthrenequinone monoimines (2,7-dinitro (**1d**), 2,7-dibromo (**1c**), and 2,7-di-*tert*-butyl (**1a**)) show a decreasing reaction rate in the listed order, while the CVs of the quinone monoimines **1a–d** exhibited an increasing reduction potential E^0_{pc} in CH_3CN, **1a** = −0.955, **1b** = −0.885, **1c** = −0.698 and **1d** = −0.558 V (50 mV s^{-1} scan rate, Fc/Fc^+ internal standard, 0.1 M) (Fig. S6, ESI†). This is in agreement with the assumption that with a higher oxidation potential of the quinone imines (**1**) a faster reaction rate is observed (Table 1).

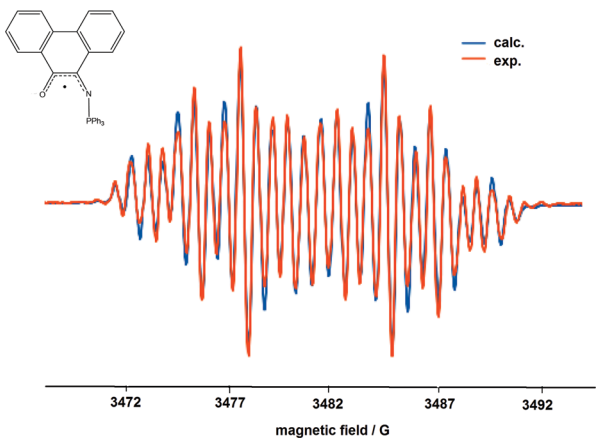

Fig. 2 The X band EPR spectrum from **1b** and triphenylphosphine (measured – red and simulated – blue). Parameters: g = 2.0032, a_P = 6.90, a_N = 1.10, a_{H1-7} = 2.35, 2.26, 2.11, 0.85, 0.79, 0.73, 0.67, a^{13}_C 1.5336 and 2.987G.

Table 1 The redox potentials of the imines (**1a–d**) and 1,3,2-oxazaphospholes (**3a–d**)[a]

Entry			R	$E^0_{1/2}$ (**1a–d**) (V)	$E^0_{1/2}$(**3a–d**) (V)	10^4 V_{in}[b] (Ms^{-1})
1	**1a**	**2a**	*t*Bu	−0.955	0.032	1.28
2	**1b**	**2b**	H	−0.885	0.083	1.45
3	**1c**	**2c**	Br	−0.698	0.213	—
4	**1d**	**2d**	NO_2	−0.558	0.351	18

[a] In MeCN, *tert*-butylammonium perchlorate as a supporting electrolyte, scan speed 50 mV s^{-1}, referenced to Ag/AgCl, glassy carbon and platinum electrodes. [b] [2,7-R-PQI] = 0.25 mM, [PPh_3] = 10 mM in 4 mL CH_3CN at 25 °C under Ar.

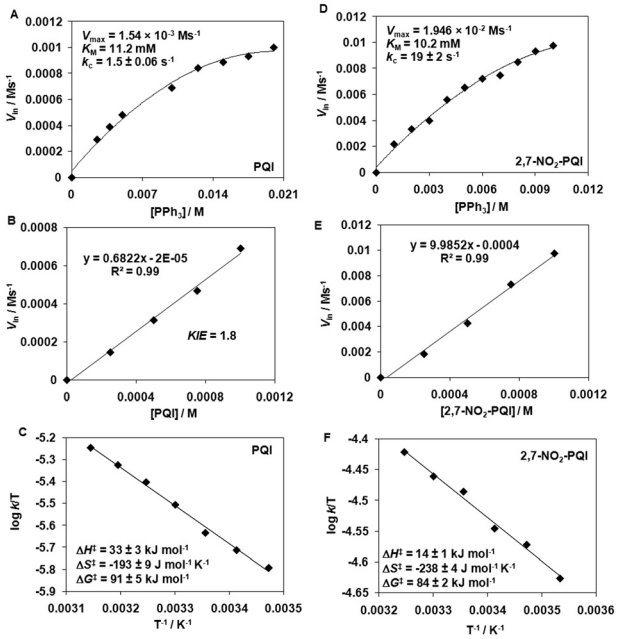

Fig. 3 Reactions of 2,7-R-PQI derivatives with PPh_3 in CH_3CN under Ar. (A) V_{in} *versus* $[PPh_3]_0$ for the formation of **3b**• at 25 °C ([**1b**] = 1 mM). (B) V_{in} *versus* $[\mathbf{1b}]_0$ for the formation of **3b**• at 25 °C ($[PPh_3]$ = 10 mM). (C) Eyring plot for the formation of **3b**•. (D) V_{in} *versus* $[PPh_3]_0$ for the formation of **3d**• at 25 °C ([**1d**] = 1 mM). (B) V_{in} *versus* $[\mathbf{1d}]_0$ for the formation of **3d**• at 25 °C ($[PPh_3]$ = 10 mM). (C) Eyring plot for the formation of **3d**•.

N-Methyl- and *N*-phenyl-9,10-phenanthrenquinone monoimine did not react with triphenylphosphine under the same conditions, indicating that the hydrogen on the N-atom seems to have a special role in this reaction. Phenanthrenequinone monoxime reacted with triphenylphosphine in acetonitrile under argon at room temperature and yielded triphenylphosphine oxide (proved by IR $\nu(P–^{16}O)$ = 1191 cm^{-1}, ^{31}P-NMR 23 ppm and UV-vis spectroscopy (Fig. S7, ESI†)) and 9,10-phenanthrene quinone monoimine (ν(N–H) = 3200 cm^{-1}) (Fig. S8, ESI†). Detailed kinetic studies on the reaction of **1b** (0.25–1 mM) with triphenylphosphine (2.5–20 mM) were carried out in CH_3CN at 15–45 °C, and the formation (decay) of the radical was followed as an increase (decrease) in absorbance at 486 nm (Fig. 3 and Tables S1 and S2, ESI†). Under these conditions, the reaction rate is directly proportional to the concentration of PQI (**1b**) and shows Michaelis–Menten type saturation kinetics with $[PPh_3]_0$ (V_{max} = 1.54(5) × 10^{-3} Ms^{-1}, K_M = 10 mM, k_c = 1.54(6) s^{-1} at 25 °C) with $\Delta H^{\ddagger}$ = 33(3) kJ mol^{-1}, $\Delta S^{\ddagger}$ = −193(9) J mol^{-1} K^{-1}, and $\Delta G^{\ddagger}$ = 91(5) kJ mol^{-1}, establishing intermediate complex (adduct) formation in an associative-type bimolecular reaction (Fig. 3A–C). A similar kinetic feature was observed for **1d** with V_{max} = 1.95(1) × 10^{-2} Ms^{-1}, K_M = 11 mM, and k_c = 19(2) s^{-1} at 25 °C with $\Delta H^{\ddagger}$ = 14(1) kJ mol^{-1}, $\Delta S^{\ddagger}$ = −238(4) J mol^{-1} K^{-1}, and $\Delta G^{\ddagger}$ = 84(2) kJ mol^{-1} (Fig. 3D–F). The activation enthalpy of 14(1) kJ mol^{-1} and the calculated Gibbs energy of 84(2) kJ mol^{-1} observed for **1d** are smaller than those observed for **1b**, which is consistent with the higher reactivity of **1d** with PPh_3 (k_{rel}(**1d**/**1b**) = 15 at 25 °C). The relative rate based on the formation and decay process (V_{form}/V_{dec}) of **2b**• is ∼12 at R.T. ([**1b**] = 1 mM; $[PPh_3]$ = 10 mM). A comparison of the reaction rates measured with H-PQI and D-PQI shows a noticeable H/D kinetic isotope effect (KIE = 1.8), demonstrating that proton transfer and/or disruption of hydrogen bonding is involved in the rate-determining step.[11]

Density functional theory (DFT) calculations were carried out to understand the formation of the radical species (ESI†). We found that neither the reaction 2 PQI → PQIH• + PQI_{-H}• (ΔG_r = 107.5 kJ mol^{-1}) nor the reaction PQI + PPh_3 → $PQI^{\bullet -}$ + $PPh_3^{\bullet +}$ (ΔG_r = 193.3 kJ mol^{-1}) was favored thermodynamically; therefore, we expected direct complex formation (Fig. S9, ESI†) by the reaction $[PQI + PPh_3]_{solvent\ cage}$ → PQI–PPh_3 (1), whose activation barrier was 77.2 kJ mol^{-1} and which resulted in a stable intermediate **I1** (−8.3 kJ mol^{-1}). This form could interact with a second PQI resulting in the experimentally observed stable **2b**• and PQIH• through stable radical pairs (Fig. S10, ESI†) in a solvent cage (2), which is thermodynamically favored (ΔG_r = −23.3 kJ mol^{-1}). After the separation of the radicals, the resting PQIH• could react with another PQIH• predicting an antiferromagnetic interaction. Taking into account the reaction between forms having stacking interactions (3), the energetics was exergonic (ΔG_r = −11.4 kJ mol^{-1}). From **I1** both the **2b** (−15.3 kJ mol^{-1}) and **3b** (−26.4 kJ mol^{-1}) products could form directly by internal hydrogen transfer or cyclization (4–5), where the latter one had a significantly lower barrier by 25.3 kJ mol^{-1}. The formation of the final products **2b** and **3b** could also occur by hydrogen transfers of the PQI derivatives; however, it was found that the reaction **2b**• + PQI → **2b** + PQI_{-H}• was strongly endergonic (ΔG_r = 126.6 kJ mol^{-1}) while the quenching by PQIH• and $PQIH_2$ was less unfavored with ΔG_r = 16.3 and 15.7 kJ mol^{-1} (6–7). Note that these values are lower by 11.1 kJ mol^{-1} in the case of **3b** (8–9); however, the latter one could be formed indirectly through **I1**. The formation of **2b** or **3b** is depending on which side of **2b**• interacts with PQIH• or $PQIH_2$. Comparing the energies of the predicted intermediates, the type of atom transfer was analyzed. We proposed SET-PT (single electron transfer-proton transfer) in the case of quenching from PQIH• and SPLET (sequential proton loss electron transfer) in the case of quenching from $PQIH_2$.

The radical complex formation of the expected open-form oxazaphospholyl radical (PQI_{-H}• + PPh_3 → **2b**•) was significantly more preferred both kinetically ($\Delta^{\ddagger}G$ = 44.0 kJ mol^{-1}) and thermodynamically (ΔG_r = −147.7 kJ mol^{-1}); however, the formation of PQI_{-H}• was very unfavored, see above. We proposed that previously **I1** formed, which is due to the relatively low activation barrier.

These results predict slow formation of the non-radical species **2b** and **3b** and the long-term existence of **2b**•.

In summary, we proposed a mechanism according to the following reactions:

$$[PQI + PPh_3]_{solvent\ cage} \rightarrow \mathbf{I1} \qquad (1)$$

$$\Delta G_r = -8.3\ kJ\ mol^{-1}$$

$$\mathbf{I1} + PQI \rightarrow [\mathbf{RP1}]_{solvent\ cage} \rightarrow \mathbf{2b}^{\bullet} + PQIH^{\bullet} \qquad (2)$$

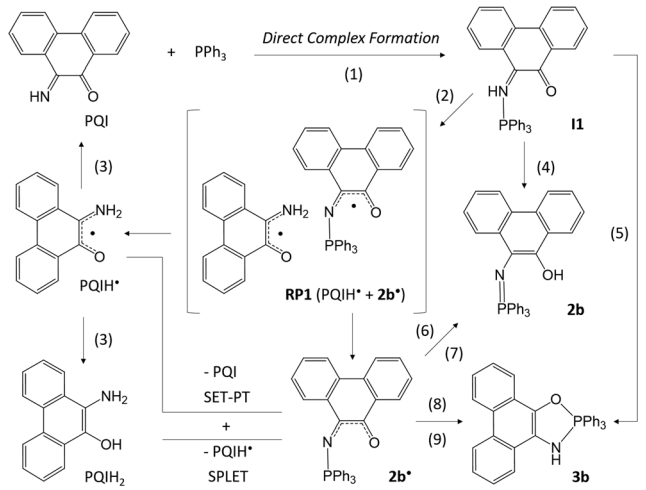

Fig. 4 Proposed mechanism of 1,3,2-oxazaphosphole formation.

$$\Delta G_r = -23.3 \text{ kJ mol}^{-1}$$
$$[\text{PQIH}^\bullet \cdots \text{PQIH}^\bullet]_{\text{stacking}} \rightarrow [\text{PQI} \cdots \text{PQIH}_2]_{\text{stacking}} \quad (3)$$

$$\Delta G_r = -11.4 \text{ kJ mol}^{-1}$$
$$\mathbf{I1} \rightarrow \mathbf{2b} \quad (4)$$

$$\Delta G_r = -7.0 \text{ kJ mol}^{-1}$$
$$\mathbf{I1} \rightarrow \mathbf{3b} \quad (5)$$

$$\Delta G_r = -11.8 \text{ kJ mol}^{-1}$$
$$\mathbf{2b}^\bullet + \text{PQIH}^\bullet \rightarrow \mathbf{2b} + \text{PQI} \quad (6)$$

$$\Delta G_r = 16.4 \text{ kJ mol}^{-1}$$
$$\mathbf{2b}^\bullet + \text{PQIH}_2 \rightarrow \mathbf{2b} + \text{PQIH}^\bullet \quad (7)$$

$$\Delta G_r = 15.7 \text{ kJ mol}^{-1}$$
$$\mathbf{2b}^\bullet + \text{PQIH}^\bullet \rightarrow \mathbf{3b} + \text{PQI} \quad (8)$$

$$\Delta G_r = 5.3 \text{ kJ mol}^{-1}$$
$$\mathbf{2b}^\bullet + \text{PQIH}_2 \rightarrow \mathbf{3b} + \text{PQIH}^\bullet \quad (9)$$

$$\Delta G_r = 4.6 \text{ kJ mol}^{-1}$$

We simulated UV-vis spectra to see which species had the best correlation to the experimental spectrum. The spectra of both $\mathbf{2b}^\bullet$ and $\text{PQIH}^\bullet$ had a similarity to the experimental spectrum but species in which PQI, $\text{PQIH}^\bullet$, and PQIH_2 bonded to $\mathbf{2b}^\bullet$ in different orientations showed better agreement and it was the same in the case of TEMPO as well (see Fig. S11, ESI†).

Conclusions

Based on detailed kinetic and spectroscopic studies and DFT calculations, a plausible mechanism has been proposed (Fig. 4).

The 9,10-phenanthrenequinone monoimine (**1b**) forms a charge-transfer complex in a fast preequilibrium process with triphenilphosphine (Michaelis–Menten kinetics) followed by the formation of a stable complex (**I1**). The end products can be formed directly from **I1** but thermodynamically the formation of the oxazaphospholyl radical is more favored. The hydrogen transfer from **I1** to the 9,10-phenanthrenequinone monoimine yields radical-pair 1 (RP1), probably *via* an electron-transfer-proton-transfer mechanism (ET-PT) based on the stoichiometry and the small KIE value.[11] Radicals of this type seem to be very stable due to the high delocalization of the unpaired electron on the large aromatic system and/or the H-bonds. The end product formation can be interpreted by slow H-atom abstraction and P–O bond formation *via* SET-PT (single electron transfer-proton transfer) in the case of quenching from $\text{PQIH}^\bullet$ and SPLET (sequential proton loss electron transfer) based on the DFT calculations. Since electron-withdrawing substituents on the imine enhance and electron-releasing substituents decrease the overall reaction rate the heterodiene acts as a Lewis acid in a normal electron-demand cycloaddition reaction. The present study allowed us to gain more insight into the mechanism of the cheletropic reaction of monoimines with PPh_3 *via* unexpected radical intermediates resulting in 2,3-dihydro-2,2,2-triphenylphenanthro[9,10-*d*]-1,3,2λ^5 oxazaphospholes, molecules that can be applied as flavoprotenin mimics and highly efficient organocatalysts for various oxidation processes.

Conflicts of interest

There are no conflicts to declare.

Acknowledgements

Financial support from the Hungarian National Research Fund (OTKA K108489 to JK), GINOP-2.3.2-15-2016-00049 (JK) and TKP2020-IKA-07 (JK) is gratefully acknowledged. This work was partially supported by the European Union and the European Social Fund through project Supercomputer, the National Virtual Lab, grant no.: TÁMOP-4.2.2.C-11/1/KONV-2012-0010 (MP).

Notes and references

1 W. L. Mock, *Cheletropic Reactions in Organic Chemistry, Pericyclic Reactions*, ed. A. P. Marchand and R. E. Lehr, Academic Press, New York, 1977, vol. 35, ch. 2, pp. 141–179.
2 (*a*) F. Ramirez, *Acc. Chem. Res.*, 1968, **1**, 168; (*b*) F. Ramirez, C. P. Smith, J. F. Pilot and A. S. Gulati, *J. Org. Chem.*, 1968, **33**, 3787; (*c*) D. Hellwinkel, W. Blaicher, W. Krapp and W. S. Sheldrick, *Chem. Ber.*, 1980, **113**, 1406.
3 (*a*) A. A. Kutyrev and V. V. Moskva, *Russ. Chem. Rev.*, 1987, **56**, 1798; (*b*) É. Balogh-Hergovich and G. Speier, *Phosphorus, Sulfur Silicon Relat. Elem.*, 1990, **48**, 223; (*c*) M. M. Sidky and M. F. Zayed, *Tetrahedron Lett.*, 1971, **12**, 2313; (*d*) M. M. Sidky, M. F. Zayed, A. A. El-kateb and I. T. Hennawy, *Phosphorus, Sulfur Silicon Relat. Elem.*, 1981, **9**, 343.
4 G. Speier, Z. Tyeklár, V. Fülöp and L. Párkányi, *Chem. Ber.*, 1988, **121**, 1685.
5 N. Bagi, J. Kaizer and G. Speier, *RSC Adv.*, 2015, **5**, 45983.
6 I. Bors, J. Kaizer and G. Speier, *RSC Adv.*, 2014, **4**, 16928.
7 G. Székely, N. Bagi, J. Kaizer and G. Speier, *New J. Chem.*, 2015, **39**, 5908.
8 (*a*) F. Neese, *ORCA an ab initio, density functional and semiempirical program package*, *Version 2.6*, University of Bonn, Bonn, Germany, 2008; (*b*) F. Neese, *J. Chem. Phys.*, 2001, **115**, 11080–11096; (*c*) F. Neese, *J. Phys. Chem. A*, 2001, **105**, 4290–4299; (*d*) F. Neese, *J. Chem. Phys.*, 2003, **118**, 3939–3948; (*e*) F. Neese, *J. Chem. Phys.*, 2005, **122**, 034107.
9 A. Rockenbauer and L. Korecz, *Appl. Magn. Reson.*, 1996, **10**, 29–43.
10 (*a*) G. Speier, *New J. Chem.*, 1994, **18**, 143; (*b*) G. Nocton, W. W. Lukens, C. H. Booth, S. S. Rozenel, S. A. Medling, L. Maron and R. A. Andersen, *J. Am. Chem. Soc.*, 2014, **136**, 8626–8641; (*c*) J. M. Wittman, R. Hayoun, W. Kaminsky, M. K. Coggins and J. M. Mayer, *J. Am. Chem. Soc.*, 2013, **135**, 12956–12959.
11 R. Tyburski, T. Liu, S. D. Glover and L. Hammarström, *J. Am. Chem. Soc.*, 2021, **143**, 560–576.